

----- supp info -----

High-throughput screening: speeding up porous materials discovery

Philipp Wollmann^a, Matthias Leistner^b, Ulrich Stoeck^a, Ronny Grünker^a, Kristina Gedrich^a, Nicole Klein^a, Oliver Throl^a, Wulf Grählert^b, Irena Senkovska^a, Frieder Dreisbach^c, and Stefan Kaskel^{a,b}

^a Department of Inorganic Chemistry; Dresden University of Technology; Bergstrasse 66, 01069 Dresden (Germany).

^b Department CVD / Process Monitoring; Fraunhofer IWS; Winterbergstrasse 28, 01277 Dresden (Germany).

^c Rubotherm GmbH, Universitätsstrasse 142, 44799 Bochum (Germany)

Supplementary Index

- 1. High-throughput screening**
- 2. Synthesis of MOFs**
- 3. Powder X-ray diffraction**
- 4. Crystal structure of new MOFs**
- 5. Thermogravimetric analyses (TGA) and infrared spectroscopy**
- 6. Adsorption measurements**

1. High-throughput screening of porous materials

The tool combines the measurement of heat of adsorption with a multiple port interface. All measurements are performed at room temperature, *n*-butane was chosen as adsorptive because of high heat of adsorption released during the adsorption process. All types of porous materials are suitable for the measurements as well as the simultaneous investigation of different materials, however a general access for *n*-butane (kinetic diameter 4.3 Å) to the pore system of porous material is required as long as *n*-butane is used. The application of other gases or vapors with smaller kinetic diameter is under investigation (another example with cyclohexane is given in part 1.5 of supporting information).

The volume of a single measuring port is below 0.1 cm³.

1.1. Measurement

Data are recorded at room temperature with a micropyrometer sensor array. *n*-Butane (purity 99.95 %) was used as adsorptive gas and nitrogen as purge gas (purity 99.999 %).

The measurement is typically completed within five minutes. As presented in figure S1, a time dependent voltage signal is recorded. The signal undergoes several statistic processes and is integrated afterwards. The sample mass (in every port) is included in data analysis – obtaining the specific heat of adsorption.

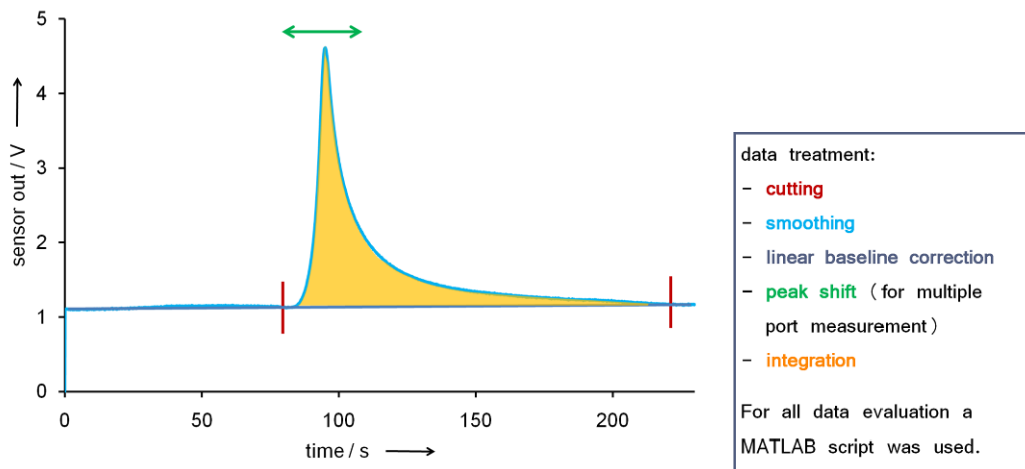


Figure S1. Data treatment of a the sensor signals

1.2. Signal statistics

Figure S2 shows a plot of integrated signals from twelve ports after the measurement on the same activated carbon. Minor deviations in signal form and course were observed. Statistic analysis proofs the correctness of the signal.

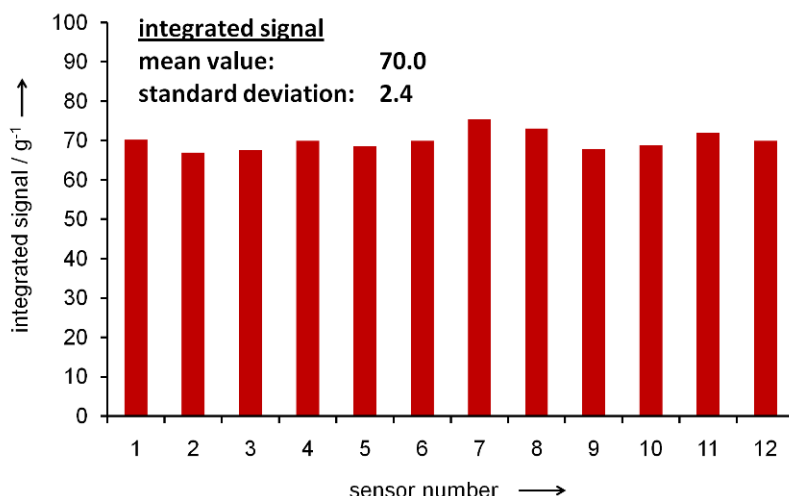


Figure S2. Signal statistics of the same activated carbon in a twelve port measurement.

1.3. Determination of *n*-butane adsorption capacity of activated carbons

The *n*-butane adsorption capacity of various activated carbons (Adsoritech GmbH, Premnitz/Germany) was determined gravimetrically using a vessel with a volume of 0.29 cm³, the mass was determined twice subsequent to the loading with activated carbon and after *n*-butane adsorption (flow: 200 ml/min, 5 min, 100 % *n*-butane). The *n*-butane capacities and *n*-butane indexes from data sheets are listed in table S1.

Table S1. Accuracy of gravimetrically determined *n*-butane adsorption capacity in comparison to *n*-butane index.

carbon nr.	1	2	3	4	5	6	7	8
<i>n</i> -butane index (data sheet)	50.01	31.4	37.5	39.5	34.9	34.6	undisclosed	undisclosed
<i>n</i> -butane capacity (gravimetric, this work)	51.6	32.0	37.1	39.4	37.5	35.0	42.7	26.7
deviation	3.1 %	1.8 %	1.0 %	0.2 %	7.4 %	1.1 %	-	-

1.4. Correlation of integrated signal with BET surface area

The integrated signal was correlated to single point BET surface areas (determined at 0.3 p/p₀).

1.5. Correlation of integrated signal with cyclohexane adsorption capacity

In addition to the adsorption of *n*-butane the performance of the high-throughput tool was also tested using cyclohexane as adsorptive on activated carbons (samples see Table S1, additional three more activated carbons were investigated). Figure S3 presents the cyclohexane adsorption (10% cyclohexane in N₂, 25 ml/min gas flow per port). Thereby, the results of the high-throughput investigations are compared with the results of cyclohexane adsorption measured gravimetrically. A correlation of 92 % of the integrated signal with cyclohexane adsorption capacities is achieved.

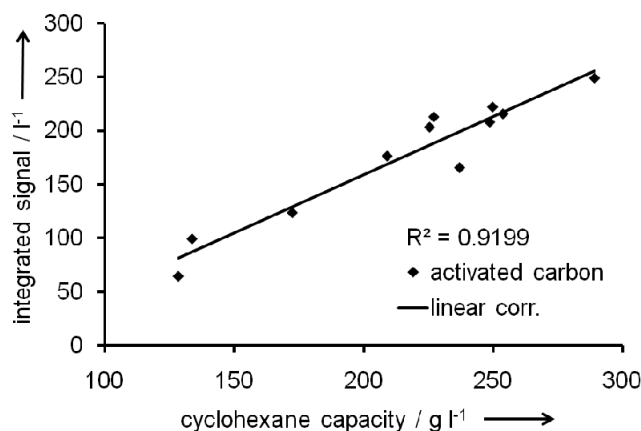


Figure S3. Correlation of cyclohexane adsorption (integrated signal) with gravimetrically determined adsorption capacity.

1.6. Signal behavior of different materials during *n*-butane adsorption

Five different commercial porous materials were chosen for examination of the performance and the applicability of the method: activated carbon, metal-organic frameworks, and a zeolite. Figure S4 demonstrates a typical measurement run for different microporous materials: Sorbonorit 3 (activated carbon, Norit GmbH, Riesbürg/Germany), Basolite C300, Basolite Z1200, Basolite A100 (all Basolite materials: BASF AG, Ludwigshafen/Germany) and ZeoCat PZ-2 (ZeoChem AG, Uetikon/Switzerland). All materials were measured simultaneously in activated state (evacuation at 150 °C for 24 h) in different ports.

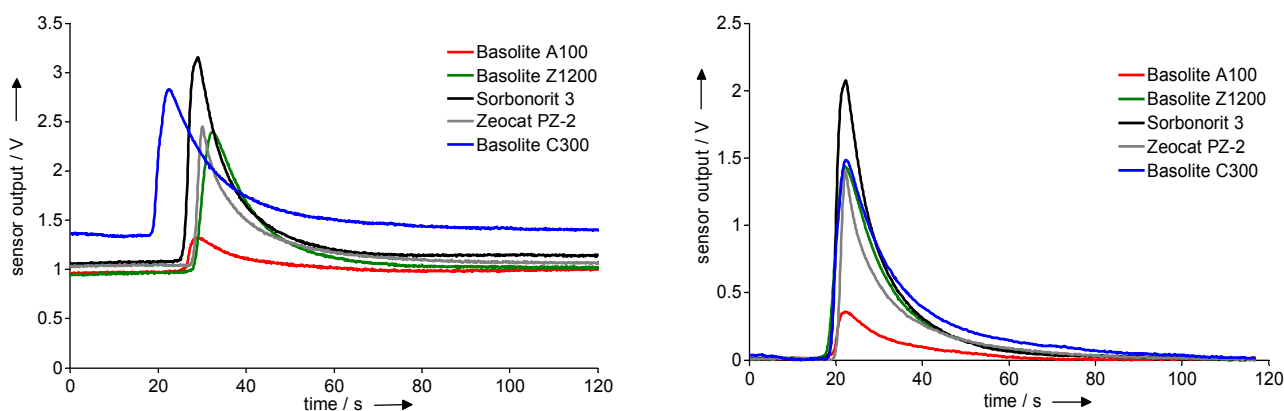


Figure S4. Sensor output for porous materials during a typical *n*-butane adsorption measurement / left: raw data; right: after data treatment.

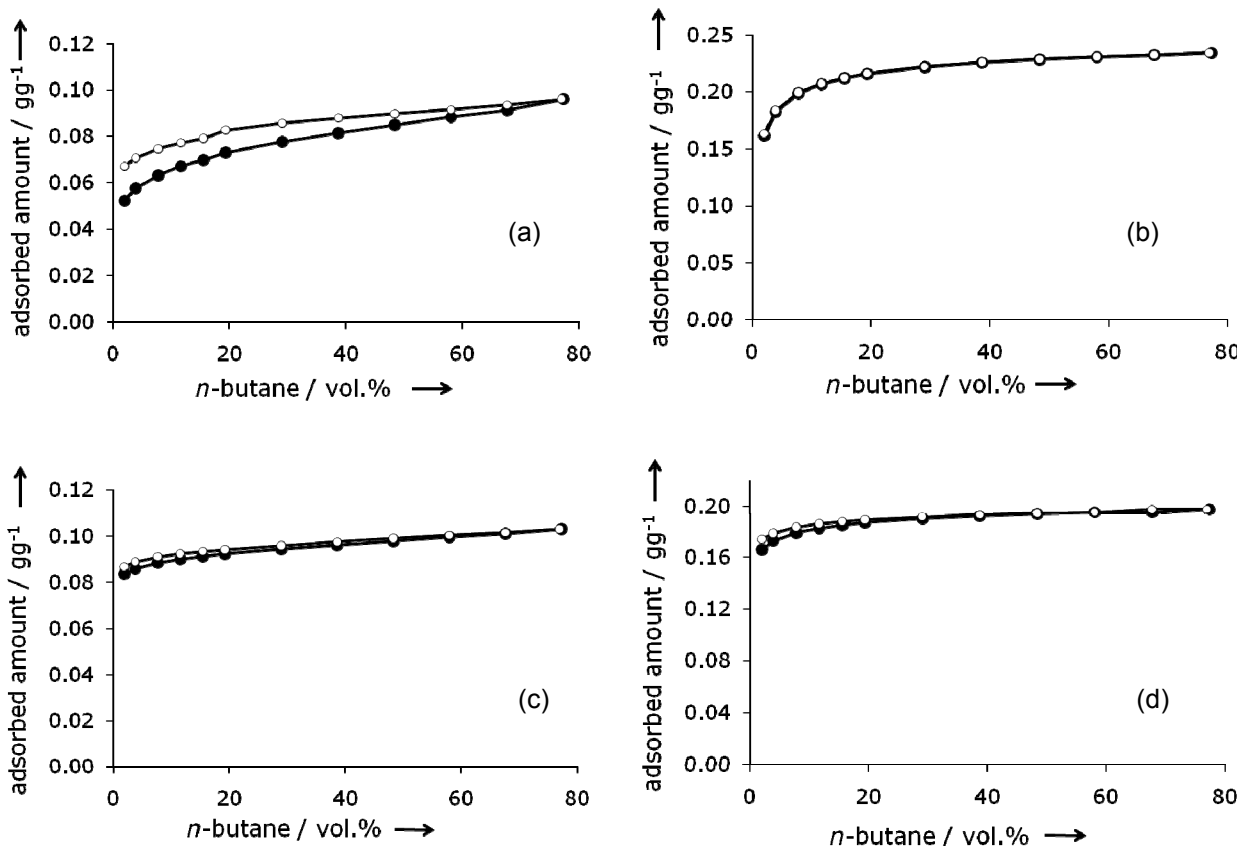
Table S2. Commercial materials used for *n*-butane adsorption experiments.

compound	pore size*	integrated signal	sample mass (mg per port)	integrated signal (per gram)
Activated Carbon Sorbonorit 3	< 10 Å	23.96	16.5	1452.1
Zeolith ZEOCat PZ-2	5.3 x 5.5 Å 5.1 x 5.5 Å	18.25	51.5	354.0
Basolite C300 ($\text{Cu}_3(\text{BTC})_2$)	5 Å / 11 Å / 13.5 Å	29.47	33.8	871.9
Basolite A100 (MIL-53 _{Al})	13.04 Å	6.30	28.7	219.1
Basolite Z1200 (ZIF-8)	11.6 Å	23.21	25.0	928.4

* according to suppliers data sheet or original literature

In table S2 the results of the high throughput screening tool are summarized. The data show, that the logging of the integral signal can give a feedback about the porosity of the materials. But it is obvious that the integrated signal depends on various factors: pore size, adsorption sites, hydrophilic/hydrophobic characteristics of the surface etc.^[1], thus different material classes lead to different correlation.

In a next step, the correlation between gravimetric *n*-butane uptake and the integrated signals of the samples was investigated. In this case, the influence of hydrophilic/hydrophobic characteristics of the materials on the measurement could be avoided. Figure S5 presents the *n*-butane adsorption isotherms of the investigated materials and gives evidence about accessibility of the pores for *n*-butane.



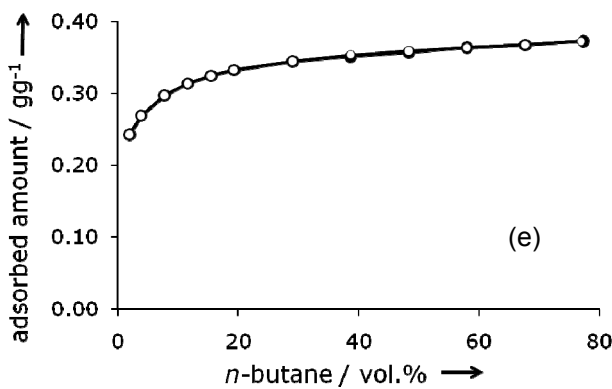


Figure S5. *n*-Butane adsorption isotherms of (a) Basolite A100, (b) Basolite Z1200, (c) ZEOCat-PZ-2, (d) Basolite C300, and (e) Sorbonorit 3 at 293K.

The *n*-butane adsorption capacities of the commercial materials at 1 bar were additionally determined gravimetrically (see part 1.3. in SI). The measured *n*-butane uptake corresponds to the *n*-butane adsorption isotherms. The obtained values (table S3) were correlated to the integrated signal achieved by Infrasorb-12, as shown in figure S6. Thereby, the quality factor R^2 is determined to 0.9765.

Table S3. Correlation of integrated signal with *n*-butane adsorption capacity.

material	mass adsorbent (g/port)	absolute <i>n</i> -butane uptake (g)	specific <i>n</i> -butane uptake (g/g)
Basolite A100 (A)	0.1017	0.0099	0.10
Basolite Z1200 (B)	0.0934	0.0232	0.25
Zeocat PZ-2 (C)	0.2192	0.0198	0.09
Basolite C300 (D)	0.0811	0.0168	0.21
Sorbonorit 3 (E)	0.0578	0.0199	0.34

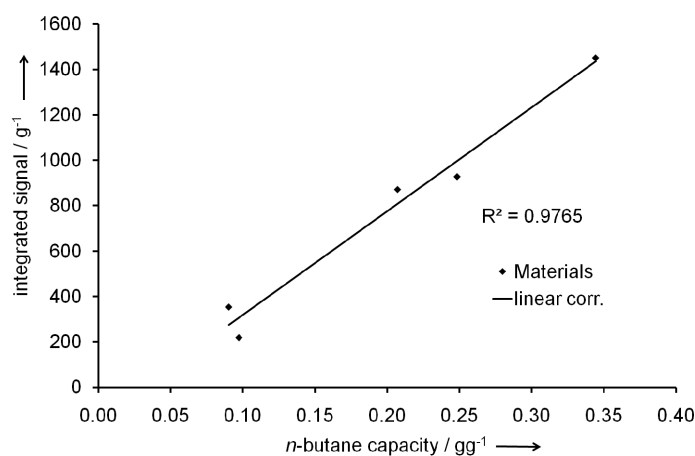


Figure S6. Correlation of integrated signal with *n*-butane adsorption capacity.

1.7. Flexible structures

As an example of a flexible network structure DUT-8(Ni)^[2] was analyzed with the Infrasorb-12. Figure S7(a) shows the *n*-butane adsorption isotherm^[2] and the resulting Infrasorb-12 signal (figure S7(b)). In general, the ability of the framework to adsorb *n*-butane (in the case of DUT-8(Ni) the opening of the framework at a certain “gate-pressure”) is required for the efficient measurement using Infrasorb-12. For the correlation between the *n*-butane capacity and surface area value, an extended data set for flexible network structures is necessary.

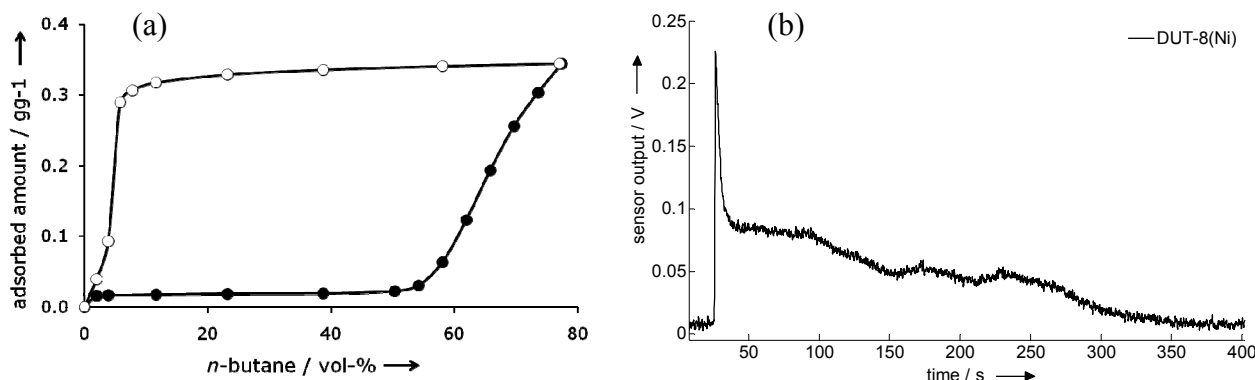
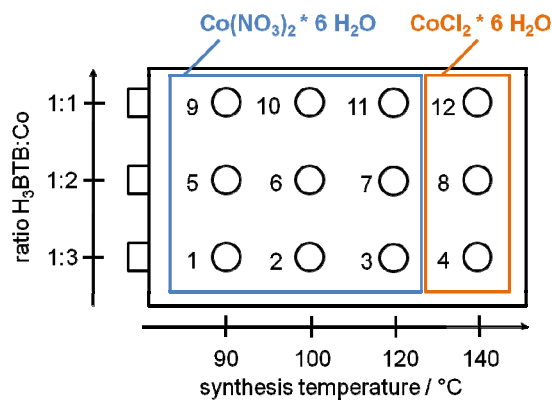


Figure S7. (a) *n*-butane adsorption isotherm of DUT-8(Ni) and (b) resulting sensor output signal in a Infrasorb-12 measurement.

The signal course of DUT-8(Ni) differs from those observed for non-flexible structures (see figure S4) due to the gate-opening effect, nevertheless the exothermic *n*-butane adsorption is clearly detectable. In principle, flexible network structures can be also measured with Infrasorb-12.

2. Synthesis of MOFs



Scheme S1. Variation of synthesis conditions, the numeration of synthesis matrix is in accordance with the measurement device.

2.1. Synthesis of Co/BTB based MOFs

H₃BTB (benzene-1,3,5-tribenzoic acid) was prepared according to literature procedures^[3,4]. Co(NO₃)₂ · 6 H₂O (Sigma-Aldrich) and CoCl₂ · 6 H₂O (Sigma-Aldrich) were used as received. N,N-dimethylformamide (DMF) and N,N-diethylformamide (DEF) were dried over phosphorous pentoxide, distilled and stored under argon.

DUT-27 (Co₂(BTB)NO₃(DEF)₃(H₂O)₂)

180 mg H₃BTB (0.41 mmol) and 367 mg Co(NO₃)₂ · 6 H₂O (1.26 mmol) were dissolved in 10.5 ml of DEF. The solution was heated in a Pyrex tube at 120° C for 20 hours. The resulting violet crystals of Co₂(BTB)NO₃(DEF)₃(H₂O)₂ were collected by filtration under argon, washed twice with DEF and dried in an argon flow at room temperature. Yield: 229 mg (59%, referring to the amount of H₃BTB). The synthesis at lower temperatures (reaction vessel 1, 2) yielded no product.

Elemental analysis for Co₂(BTB)NO₃(DEF)₃(H₂O)₂: wt% obs. ± σ (calc.): C: 52.1 ± 0.7 (52.8), H: 5.40 ± 0.09 (5.49), N: 5.8 ± 0.2 (5.9), O: 22.8 ± 0.3 (23.5), Co: 12.9 ± 0.3 (12.3). IR (cm⁻¹): 667 (m), 710 (m), 748 (w), 787 (s), 812 (m), 825 (m), 866 (m), 889 (s), 945 (w), 1016 (m), 1072 (w), 1105 (m), 1122 (m), 1182 (w), 1215 (m), 1267 (m), 1308 (w), 1385 (w), 1417 (s), 1558 (m), 1594 (m), 1649 (s), 1668 (s), 2875 (w), 2939 (m), 2978 (m), 3045 (w), 2700 - 3700 (br).

MOF-39 (Co) (Co₃O(HBTB)₂H₂O(DMF)₉)

171 mg H₃BTB (0.4 mmol) and 286 mg CoCl₂ · 6 H₂O (1.2 mmol) were dissolved in 20 ml of DMF. To the solution, 2 ml of 0.05 M aqueous tetramethylammonium hydroxide solution were added and subsequently heated in a Schott Duran thread bottle at 140° C for 3 hours. The resulting violet block-shaped crystals were collected by filtration under argon, washed twice with DMF and EtOH and dried in argon atmosphere at room temperature. Yield: 157 mg (73%, referring to the amount of H₃BTB). The synthesis at the ratios of 1:1 and 1:2 of H₃BTB to CoCl₂ · 6 H₂O (reaction vessel 8, 12) were performed in the same way.

Elemental analysis for Co₃O(HBTB)₂H₂O(DMF)₉: wt % obs. ± σ (calc.): C: 56.1 ± 0.2 (55.81), H: 6.00 ± 0.1 (5.61), N: 7.28 ± 0.09 (7.24), O: 21.8 ± 0.2 (21.13), Co: 10.2 ± 0.1 (10.15). IR (cm⁻¹): 669 (m), 707 (m), 786 (s), 792 (m), 858 (m), 863 (w), 879 (w), 935 (w), 962 (w), 1016 (m), 1058 (w), 1095 (m), 1128 (w), 1253 (m), 1282 (w), 1413 (s), 1434 (w), 1490 (m), 1496 (m), 1540 (w), 1554 (m), 1594 (w), 1606 (s), 1625 (s), 1681 (s), 1710 (w), 2798 (w), 2848 (m), 2925 (m), 3052 (w), 2700 - 3700 (br).

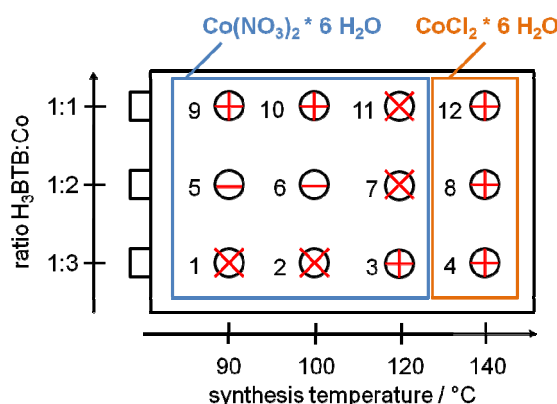
DUT-28 ($\text{Co}_{22}(\text{BTB})_{12}(\text{NO}_3)_8(\text{DEF})_x(\text{H}_2\text{O})_y$)

67 mg (0.15 mmol) H_3BTB and 45 mg (0.15 mmol) of $\text{Co}(\text{NO}_3)_2 \cdot 6 \text{ H}_2\text{O}$ were dissolved in 10 ml of DEF. The solution was transferred to a Pyrex tube and heated to 90 °C (or 100 °C respectively) for 120 hours. The obtained violet crystals were filtered off under argon, washed with DEF and dried in argon flow at room temperature. Yield: 108 mg (55 %). The synthesis in the reaction vessels 5, 6, 7 and 11 were varied in temperature and ratio H_3BTB to cobalt nitrate according to scheme S2.

Elemental analysis for $\text{Co}_{22}(\text{BTB})_{12}(\text{NO}_3)_8(\text{DEF})_x(\text{H}_2\text{O})_y$ wt% obs. $\pm \sigma$ (calc.): C: 57.6 ± 0.1 (56.8), H: 7.5 ± 0.3 (6.7), N: 8.2 ± 0.3 (7.4), O: 20.5 ± 0.2 (19.7), Co: 7.6 ± 0.3 (7.8) IR (cm^{-1}): 667 (m), 703/705 (m), 725 (w), 784 (s), 808/809 (m), 860 (m), 879 (w), 941 (m), 993 (w), 1016 (m), 1070 (w), 1081 (w), 1105 (m), 1135 (w), 1178 (m), 1214 (m), 1263 (m), 1301 (m), 1363 (w), 1415 (s), 1434 (w), 1452 (w), 1496 (w) 1550 (m), 1594 (w), 1612 (w), 1646 (w), 1675 (s), 2755 (w), 2871 (w), 2933 (m), 2975 (m), 3058 (w), 2700 - 3700 (br).

2.2. Screening of synthesized MOFs

The reactant ratio leads to product formation in the reaction vessels 3-6, 8-10 and 12. For the combinations in 1, 2, 7 and 11 no product is obtained. The products in vessels 5 and 6 are highly contaminated by a grayish X-ray amorphous powder (DUT-28 was also detected). Further investigations of these products were not performed. After synthesis and activation the MOFs are handled under inert atmosphere.



Scheme S2. Variation of synthesis conditions and obtained products (x – no product obtained, - product and contaminations, + single phase product).

Table S4. Numerical values of integral signal for Co-BTB fast screening.

material	integral signal (g^{-1})
port 3	0.46
port 4	0.54
port 8	0.20
port 9	4.51
port 10	4.24
port 12	0.37

3. Powder X-ray diffraction

Powder X-ray diffraction patterns (PXRD) were collected in transmission geometry (Debye-Scherrer geometry for DUT-28) with a STOE STADI P diffractometer operated at 40 kV and 30 mA with monochromated Cu-K α_1 ($\lambda = 0.15405 \text{ nm}$) radiation and with a scan speed of 30 s/step and a step size of 0.1° .

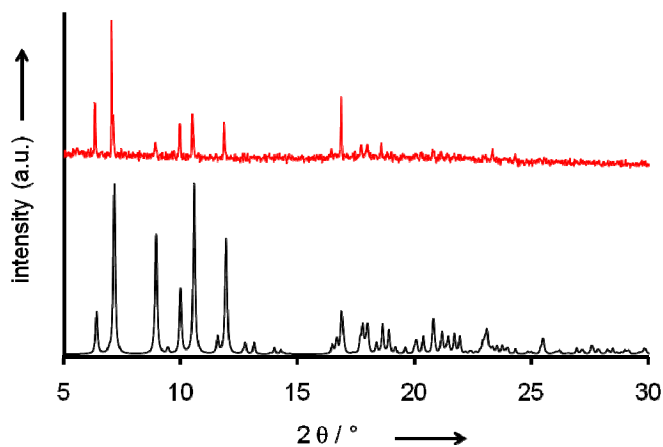


Figure S8. Measured powder X-ray diffraction pattern of the as-synthesized material (red) and calculated (from single crystal data, black) of DUT-27.

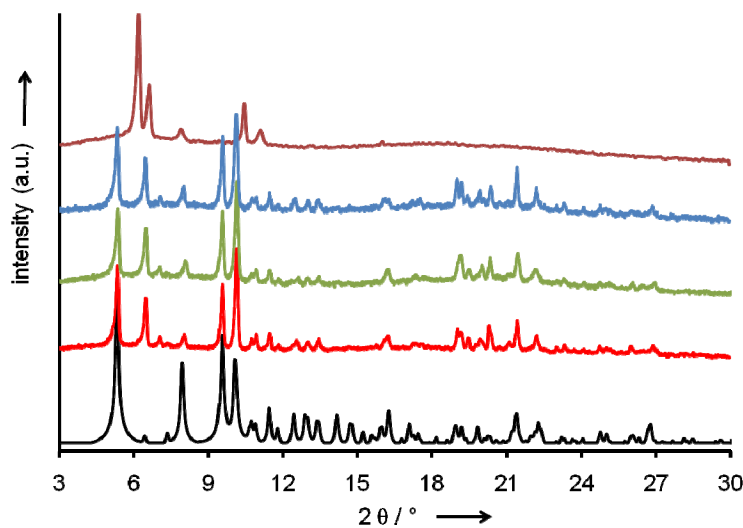


Figure S9. Measured powder X-ray diffraction patterns of the as-synthesized MOF-39(Co) (port 4 - red / port 8 – green / port 12 – blue), calculated from single crystal data (black) and after supercritical drying (port 4, dark red). The diffraction patterns of the substances in port 8 and 12 are identical (data not shown).

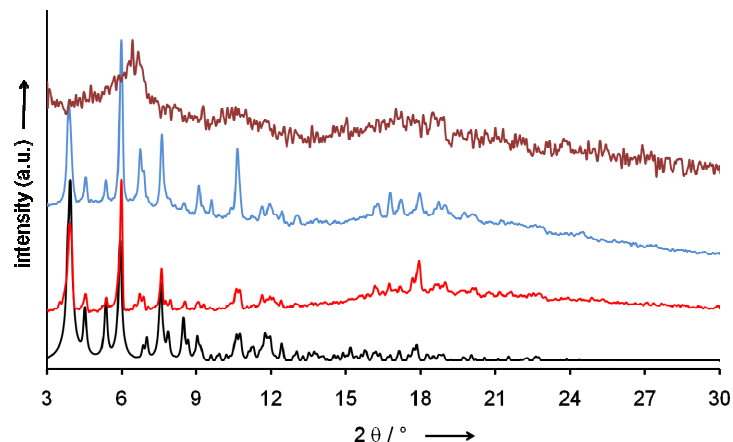


Figure S10. Measured powder X-ray diffraction pattern (room temperature) of DUT-28 as-synthesized (port 9 – red / port 10 - blue), calculated from single crystal data (black), and after supercritical drying (port 9, dark red). The diffraction patterns of the supercritical dried substance from port 10 and 9 are identical (data not shown).

4. Crystal structure

The crystal of DUT-27, DUT-28, MOF-39(Co) respectively, was sealed in a glass capillary with a small amount of solvent. The data for DUT-27 and DUT-28 were collected at 20 °C using synchrotron radiation on beamline BL14.2 of the Joint Berlin-MX Laboratory at BESSY-II (Berlin, Germany) with a MX-225 CCD detector (Rayonics, Illinois). An additional measurement was performed on DUT-28 crystal at 100 K. Integration and scaling of the data were performed with XDS program package.^[5] For MOF-39(Co), the intensity data set was collected on a Bruker X8 ApexII 4 K Kappa CCD diffractometer using Mo-K α radiation. The structures of DUT-27 and DUT-28 were solved using direct methods with the help of SHELXS-97^[6] and the structure of MOF-39(Co) using charge-flipping algorithm with the help of SUPERFLIP^[7] and refined by full-matrix least squares techniques using SHELXL-97.^[8] Non-hydrogen

atoms of the networks were refined with anisotropic temperature parameters. The hydrogen atoms of the linker molecules were geometrically constrained. Due to the low residual electron density and strong disorder it was impossible to locate the guest molecules in the crystal structures. The coordinated DEF and H₂O molecules could be positioned in DUT-27. Application of the SQUEEZE^[9] routine in the PLATON software package produced a new intensity data set excluding the intensity contribution from disordered solvent molecules.

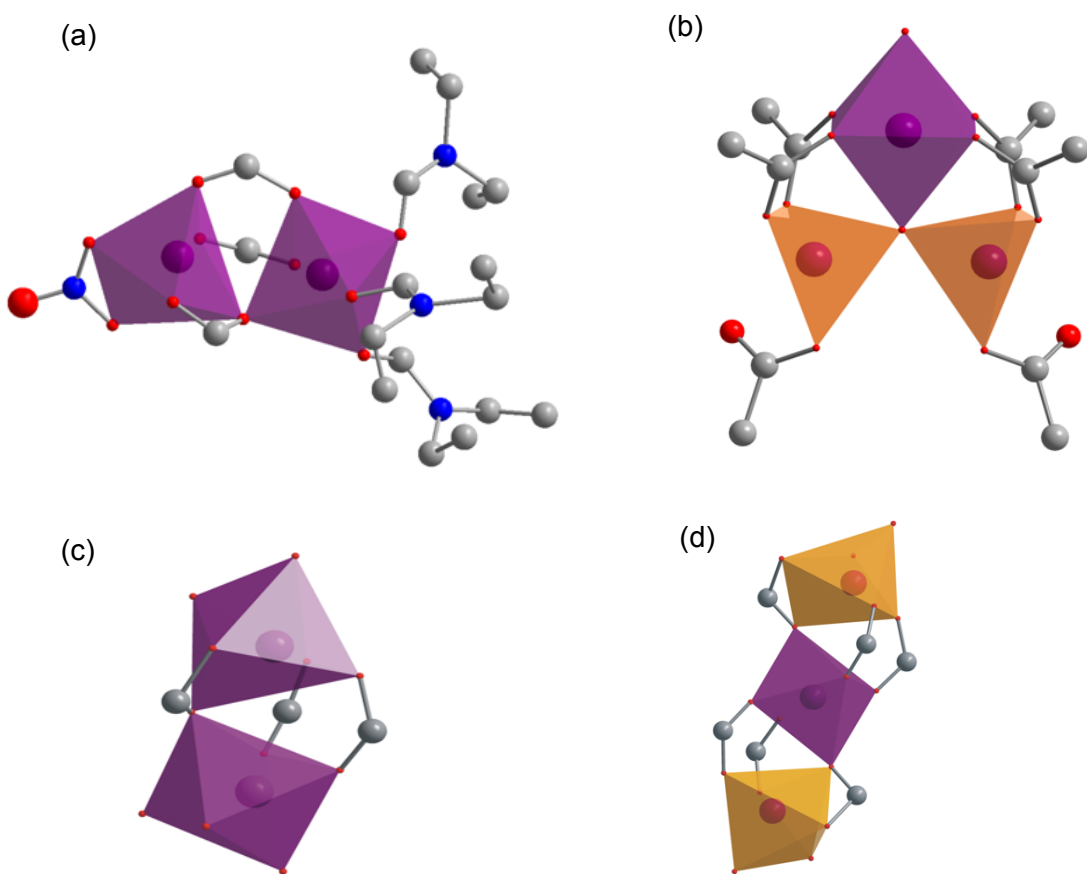
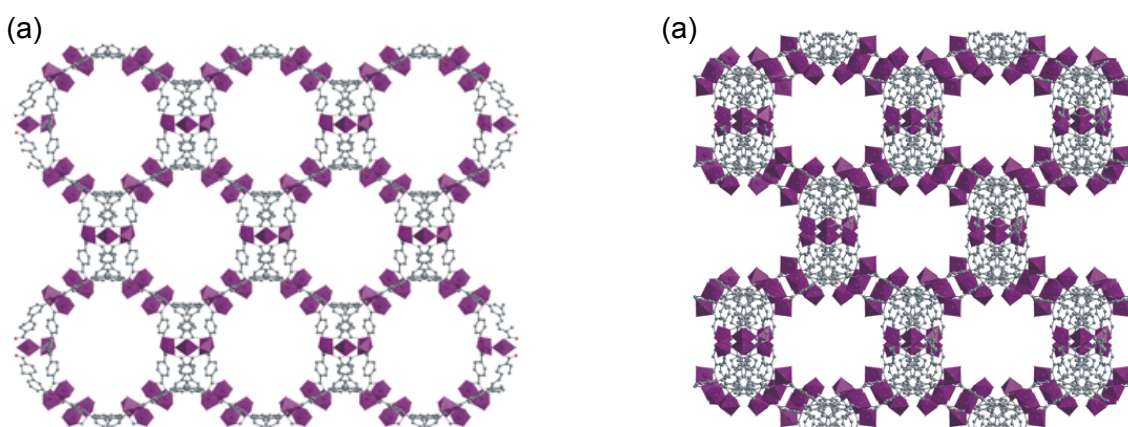


Figure S11. (a) Co₂(COO)₃(NO₃) cluster in Co₂(BTB)NO₃(DEF)₃ (DUT-27); (b) Co₃O(COO)₆ cluster in Co₃O(HBTB)₂ (MOF-39(Co)); (c) Co₂(COO)₃ cluster and (d) Co₃(COO)₆ cluster in [Co₁₁(BTB)₆]⁴⁺ (DUT-28).



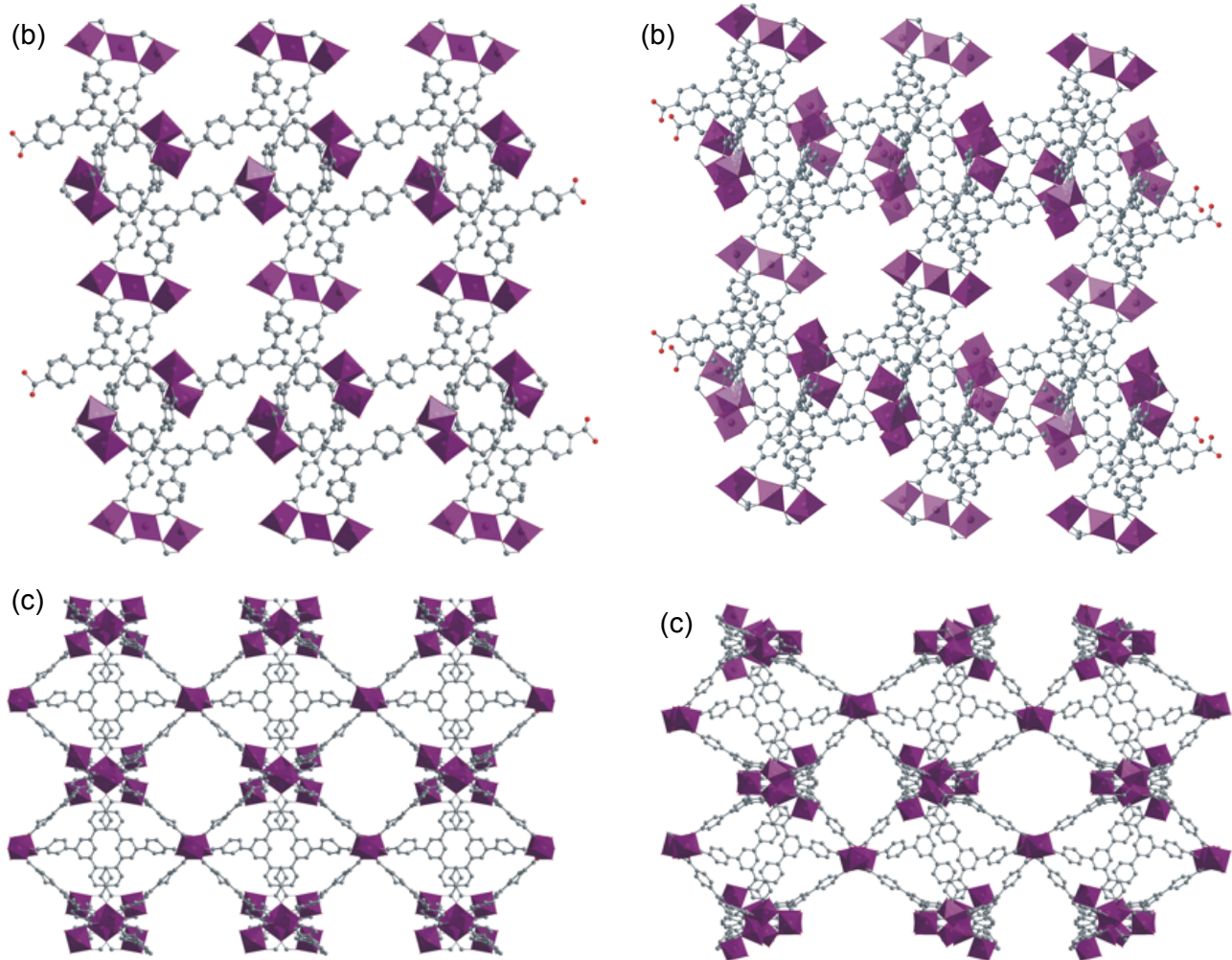


Figure S12. Structure of DUT-28; left column: room temperature structure / right column: cryogenic structure; view along a) [001], b) [010], c) [001].

5. Thermogravimetric analyses (TGA) and infrared spectroscopy

TGA were carried out under air atmosphere using a Netzsch STA 409 thermal analyzer. Infrared spectra (IR) for general compound characterization were recorded in diffuse reflection geometry (PIKE Easy Diff, Pike Technologies; Madison/WI; USA) using a Nicolet Magna 550 Series 2 infrared spectrometer (Thermo Fisher Scientific Inc.; Waltham/MA; USA) in a resolution of 4 cm^{-1} .

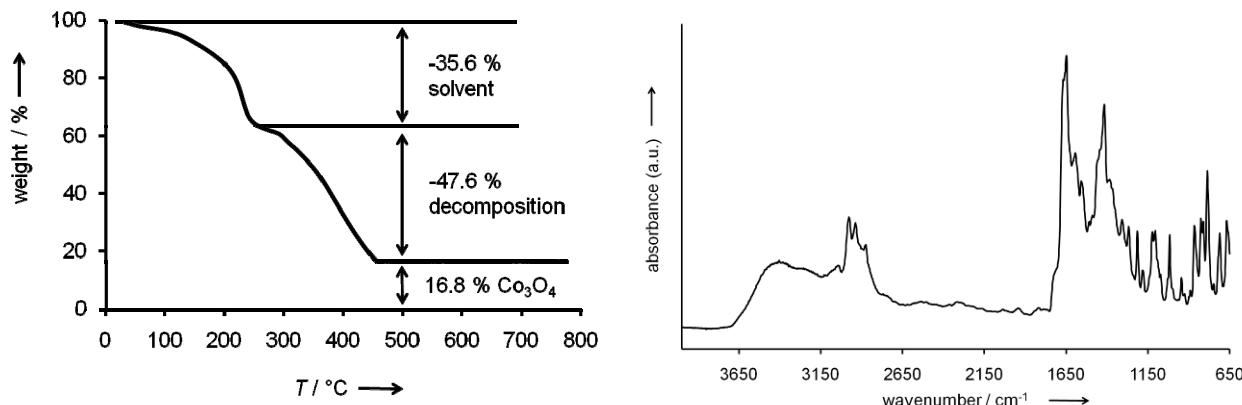


Figure S13. (a) TGA and (b) infrared spectrum of DUT-27 dried in an argon flow.

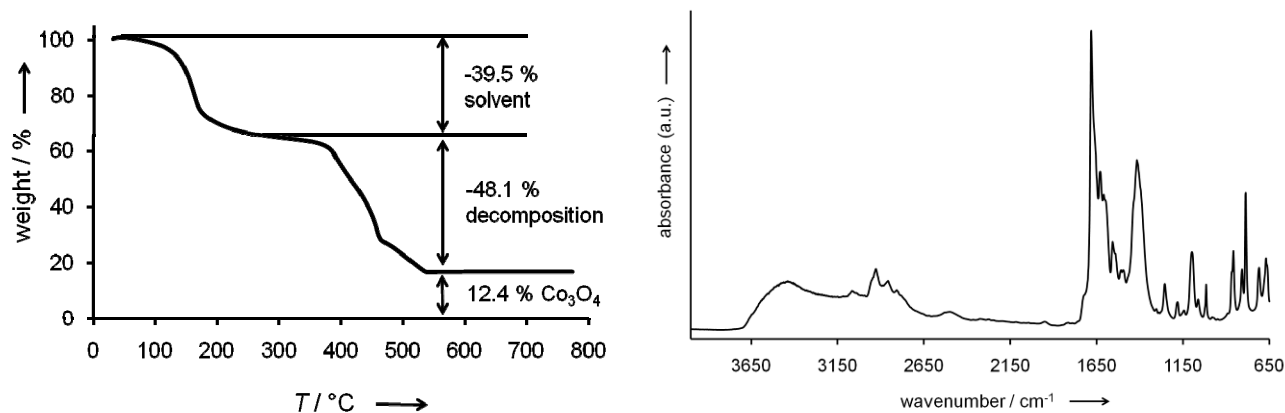


Figure S14. (a) TGA and (b) infrared spectrum of MOF-39 (Co) dried in argon flow.

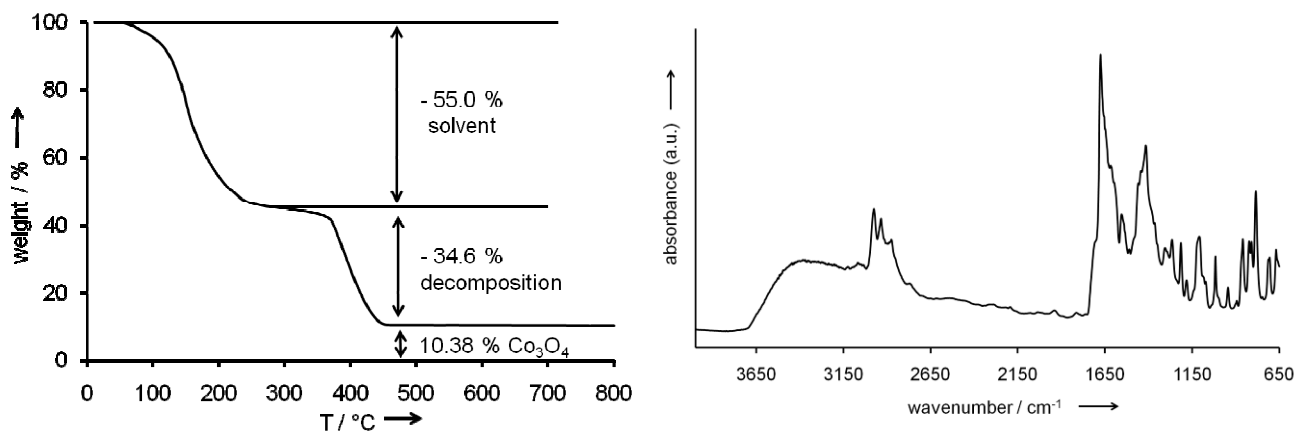


Figure S15. (a) TGA and (b) IR spectrum of DUT-28 dried in argon flow.

Anion-binding in DUT-28

According to the single-crystal analysis, the framework of DUT-28 has a positive charge. The counter ions (nitrate) could not be located. To identify the nitrate anion and the binding state in DUT-28, infrared spectra were measured on a BRUKER Vertex 70 in middle-infrared range in transmission mode (cobalt nitrate hexahydrate) or with the help of a golden gate ATR-unit (DUT-27, DUT-28; Specac Limited, Slough/USA) with a resolution of 2 cm^{-1} . All data were evaluated with BRUKER Opus 6.5 software (conversion transmission to absorbance). The cobalt nitrate hexahydrate should exhibit a band corresponding to the “free” ionic binding mode of nitrate ions. For comparison a spectrum of DUT-27, with covalent binding of nitrate groups to cobalt was recorded.

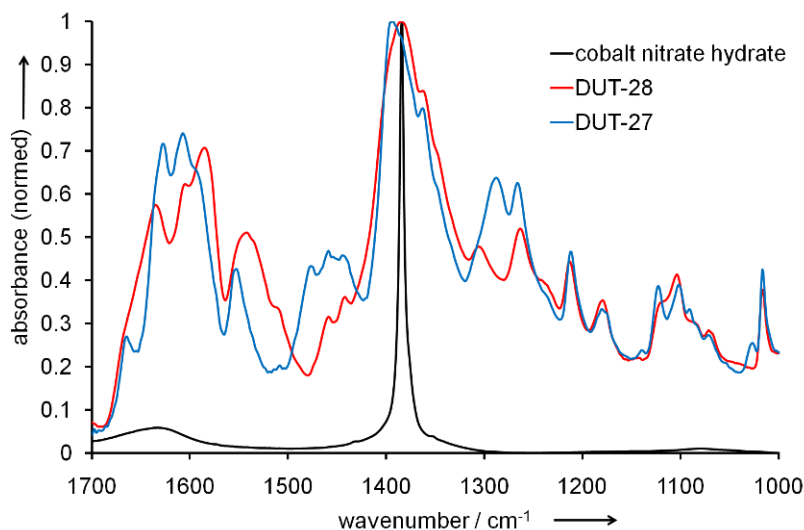


Figure S16. infrared spectra of DUT-27, DUT-28 and cobalt nitrate hydrate.

The inorganic nitrate group can be indicated easily by a very strong vibration (asymmetric stretching) at $1370\text{-}1400\text{ cm}^{-1}$ for different nitrate salts^[10,11]. For cobalt nitrate hexahydrate a very sharp peak was observed at 1384 cm^{-1} (figure S16, table S5). According to literature^[12], the value indicates the “free” ionic binding of the nitrate group in $[\text{Co}(\text{H}_2\text{O})_6](\text{NO}_3)_3$. The vibration for ionic (but solvent free) binding mode of nitrate in $\text{Co}(\text{NO}_3)_3$ is reported to have a slight shift in the observed frequency to 1389 cm^{-1} ^[12]. The nitrate band in DUT-27 is shifted in comparison to cobalt nitrate to higher wavelengths and is observed at 1393 cm^{-1} . The shift provides a spectroscopic indication for the covalent binding mode of nitrate in DUT-27 (proved by single crystal investigations). The double asymmetric stretching vibration of the chelating nitrate at 1287 cm^{-1} gives the spectroscopic evidence for the covalent binding in DUT-27^[13]. Additionally, a weak shoulder at 1384 cm^{-1} reveals also a small amount of “free” nitrate present in the compound. In opposite, the IR-spectrum of DUT-28 shows the nitrate peak at 1384 cm^{-1}

and misses the chelating-vibration at 1287 cm^{-1} . Thus, the nitrate anion in DUT-28 is in a “free” ionic binding mode and located in the pores of the framework.

Table S5. Wavenumbers of nitrate group in investigated materials.

material	wavenumber / cm^{-1} $\nu_{\text{asymm}}(\text{NO}_3^-)$
DUT-27	1393
DUT-28	1384
cobalt nitrate hexahydrate	1384

6. Adsorption measurements

N_2 physisorption isotherms were measured at 77 K up to 1 bar using a Quantachrome Autosorb 1C apparatus. Adsorption of *n*-butane was measured with a micro-balance (B111, Setaram) at 293 K and atmospheric pressure under dynamic conditions (*n*-butane diluted with nitrogen).

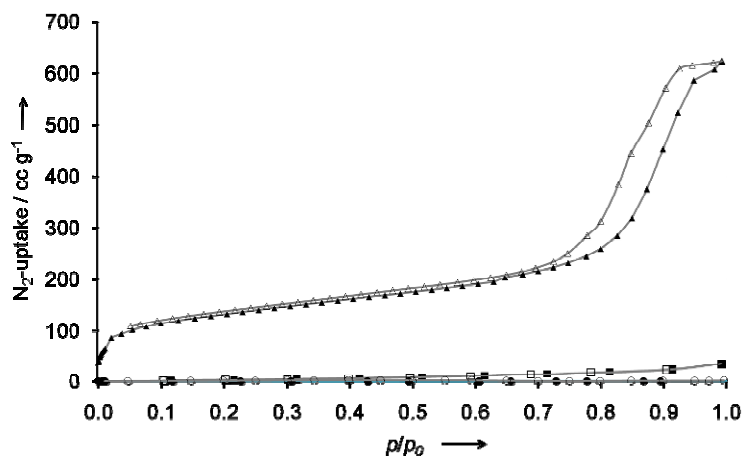


Figure S17. Nitrogen adsorption (filled symbols) and desorption (empty symbols) isotherm of DUT-28 (triangle), DUT-27 (square), and MOF-39(Co) (circle) at 77 K.

1. F. R. J. Roquerol, K Sing, *Adsorption by Powders and Porous Solids*, Academic Press Inc, 1999
2. N. Klein, C. Herzog, M. Sabo, I. Senkovska, J. Getzschmann, S. Paasch, M.R. Lohe, E. Brunner and S. Kaskel, *Phys. Chem. Chem. Phys.*, 2010, **12**, 11778-11784
3. J. Palomero, J. A. Mata, F. Gonzalez and E. Peris, *New J. Chem.*, 2002, **26**, 291-297.
4. M. V. Vasylyev and R. Neumann, *J. Am. Chem. Soc.*, 2004, **126**, 884-890.
5. W. Kabsch, *Journal of Applied Crystallography*, 1993, **26**, 795-800.
6. G. M. Sheldrick, University of Göttingen, Germany, 1997.
7. L. Palatinus, G. Chapuis, *J. Appl. Cryst.* **2007**, *40*, 786-790.
8. G. M. Sheldrick, University of Göttingen, Germany, 1997.
9. P. Van der Sluis, A. L. Spek, *Acta Crystallogr. Sect. A* **1990**, *A46*, 194-201.
10. F. A. Miller, C. H. Wilkins, *Anal. Chem.*, 1952, **24(8)**, 1253-1294
11. M. Hesse, H. Meier, B. Zeeh, *Spektroskopische Methoden in der organischen Chemie*, Georg Thieme Verlag, 1979
12. C. Ehrhardt, M. Gijkaj, W. Brockner, *Thermochim. Acta*, 2005, **432**, 36-40
13. N. F. Curtis, Y. M. Curtis, *J. Chem. Soc.*, 1965, **4(6)**, 804-809